High-efficiency and high sensitivity thermal neutron detectors based on hexagonal BN epilayers

A. Maity, S. J. Grenadier, J. Li, J. Y. Lin, and H. X. Jiang[a)]

Department of Electrical and Computer Engineering, Texas Tech University, Lubbock, TX 79409

ABSTRACT

Solid-state thermal neutron detectors with improved detection efficiencies and sensitivities are highly sought after for the detection of special nuclear materials (SNM). Due to the inherent nature of low flux of fission neutron emission from a potential SNM as well as the fact that the neutron flux is inversely proportional to the square of the distance from the SNM source, it is challenging in many cases to detect neutron signals at relatively large distances. Consequently, large size high efficiency detectors are desired to improve the detector performance and to provide a reasonable count rate (or sensitivity). We report here the successful synthesis by MOCVD of freestanding ^{10}B enriched hexagonal boron nitride (*h*-BN) epilayers with a thickness of about 50 microns. The progress towards the realization of vertical photoconductor-like thermal neutron detectors with the detector area increasing from 1 mm × 1 mm to 3 mm × 3 mm while upholding a record high detection efficiency of about 53% among solid-state neutron detectors is described. The effects of resistivity, dark current density, and the carrier mobility-lifetime products on the device performance were monitored and optimized via MOCVD growth parameters. With improved material quality, the noise related dark counts have been significantly reduced. The work laid the basis for realizing large area detectors. Our results indicate that *h*-BN epilayers are highly promising for realizing sensitive solid-state thermal neutron detectors with expected advantages resulting from semiconductor technologies, including compact size, light weight, low operating voltage, and low cost.

Key words: Solid-state neutron detectors, hexagonal boron nitride, wide bandgap semiconductors, MOCVD epitaxial growth

1. INTRODUCTION

Special nuclear materials (SNM) like Plutonium-239 (^{239}Pu) emit fast neutrons (^1_0n) through fission reactions. Thus, an effective way to detect SNM is to detect neutrons emitted by SNM. Currently, the most deployed detectors for detecting SNM are ^{3}He gas detectors. However, not only are ^{3}He gas detectors bulky, hard to configure, and require high voltage operation, but they are expensive. Thus, there has been a continuing effort to develop solid-state neutron detectors that have the performance approaching that of ^{3}He gas detectors without their drawbacks [1-12]. Potential applications of solid-state neutron detectors are numerous and include fissile materials sensing for security, neutron therapy for medical imaging, and neutron scattering and imaging for material and protein structures exploration [11]. Presently, the most effective solid-state detector approach has been the micro-structured semiconductor neutron detector (MSND) [1-4]. This type of indirect conversion detector is composed of Si filled with either ^{10}B or ^{6}LiF. The detection efficiency depends upon microstructure design, material choice, and depth of the reacting material. The most efficient semiconductor based thermal neutron detector that has ever been reported consisting of a ^{10}B filled Si microstructure with an efficiency of 48.5% [1, 2]. On the other hand, stacked ^{6}LiF filled Si detectors [4] with a certified detection efficiency of about 30% have already been commercialized by Radiation Detection Technology, Inc.

Hexagonal boron nitride (*h*-BN) epitaxial layers (epilayers), an emerging wide band gap semiconductor with an energy bandgap of Eg ~ 6.5 eV [13-20], has been explored for its deep ultraviolet photonic device applications [13-26] and its two dimensional nature [27-30]. It has a promising future in solid-state neutron detection as well [8-10]. Neutron detectors of 1 × 1 mm^2 in size fabricated from ^{10}B enriched h-BN (h-^{10}BN)

Hard X-Ray, Gamma-Ray, and Neutron Detector Physics XIX, edited by Arnold Burger, Ralph B. James, Michael Fiederle, Larry Franks, Stephen A. Payne, Proc. of SPIE Vol. 10392, 103920L
 · doi: 10.1117/12.2271556

epilayers have demonstrated the highest thermal neutron detection efficiency to date among solid-state neutron detectors at 51.4% [9]. The working principle of BN thermal neutron detectors are based on the fact that boron-10 (^{10}B) isotope has a large capture cross-section of 3840 barns for thermal neutrons [11]. When a ^{10}B atom captures a neutron, it undergoes the following nuclear reaction:

$$^{10}_{5}B + {}^{1}_{0}n = {}^{7}_{3}Li^{*}\ (0.84\ MeV) + {}^{4}_{2}\alpha^{*}\ (1.47\ MeV)\ [94\%\ excited\ state] \quad (1a)$$

$$^{10}_{5}B + {}^{1}_{0}n = {}^{7}_{3}Li\ (1.015\ MeV) + {}^{4}_{2}\alpha\ (1.777\ MeV)\ [6\%\ ground\ state] \quad (1b)$$

$$\text{Li, } \alpha \rightarrow \text{N } (e^{-}) + \text{N } (h^{+}). \qquad \text{N} \sim 10^{5} \quad (2)$$

The detection of neutrons by an h-BN detector is accomplished by two sequential processes. The first is the neutron capture of Eq. (1) in which the nuclear reaction creates Li and α daughter particles with large kinetic energies. The second process of Eq. (2) is the subsequent charge carrier generation by Li and α particles and electrons (e^{-}) and holes (h^{+}) collection, which resembles the process in a semiconductor alpha particle detector. In BN detectors, the two sequential processes described by Eqs. (1) and (2) occur in the same BN layer, making high detection efficiency possible.

^{10}B has a cross-section (σ) of 3840 barns (3.84×10^{-21} cm^2) for thermal neutrons (25 meV energy). The density of boron in *h*-BN is 5.5×10^{22} cm^{-3}. Thermal neutrons therefore have an absorption coefficient of $\alpha = N\sigma = 5.5 \times 10^{22} \times 3.84 \times 10^{-21} = 211.2$ cm^{-1} in 100% ^{10}B enriched *h*-BN (*h*-^{10}BN) films and hence the absorption length (λ) of thermal neutrons in *h*-^{10}BN can be obtained as $\lambda = 1/\alpha$ = 1/211.2 cm = 4.73×10^{-3} cm = 47.3 μm. The variation of the theoretical detection efficiency (or the thermal neutron absorption probability) of an *h*-^{10}BN detector with its thickness, d, can be expressed as

$$P(d) = 1 - e^{-d/\lambda}. \quad (3)$$

Eq. (3) is plotted in Fig. 1(a) [9]. It can be seen that at a thickness of 70 μm, *h*-^{10}BN detectors in principle can achieve a detection efficiency of 78%, which is comparable to the detection efficiency of state-of-the-art pressurized ^{3}He gas detectors. At a thickness exceeding 200 μm, *h*-^{10}BN detectors in principle can achieve a detection efficiency of 100%. Furthermore, freestanding h-BN epilayers are flexible [9], enabling the possibility for constructing detectors with versatile form factors. Moreover, due to its large band gap of about

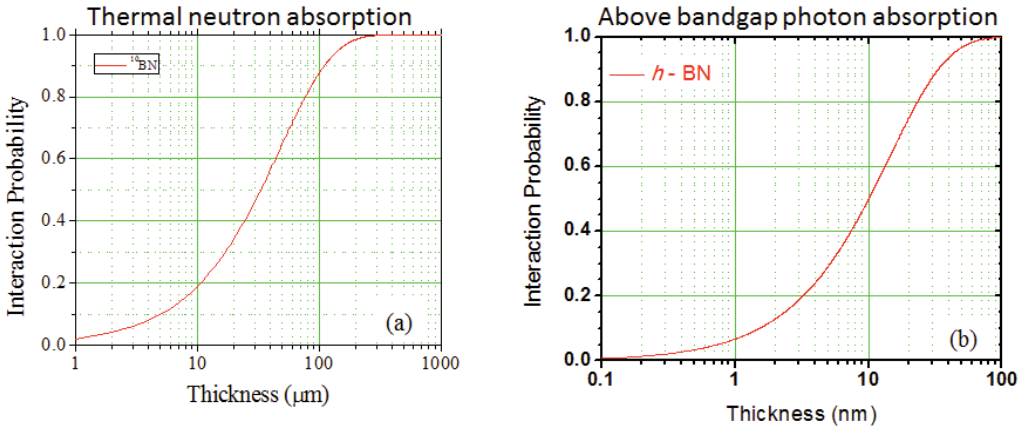

Figure 1. (a) Plot of the theoretical detection efficiency or the thermal neutron interaction probability for 100% ^{10}B enriched *h*-BN with respect to film thickness according to Eq. (3) [9]. (b) Plot of the above bandgap photon absorption probability for *h*-BN with respect to film thickness according to $P_{photon} = 1\text{-}e^{-d/\lambda}$, where λ_{photon} = 14.5 nm [26].

6.5 eV, the electrical resistivity of intrinsic h-BN well exceeds 10^{20} Ω·cm. This property is expected to provide a very low dark current density. Compared to B_4C [5], pyrolytic or polycrystalline BN [12], and alpha rhombohedral boron complexes [6, 7], *h*-BN has a simpler crystalline structure and hence epilayers produced by techniques such as metal organic chemical deposition (MOCVD) possess higher crystalline quality and fewer defect-traps, providing excellent charge transport properties. The constituent atoms of BN have low atomic numbers, making it insensitive to gamma photons [9].

2. EXPERIMENT

Epilayers of ^{10}B enriched (99.9%) *h*-BN up to 50 μm in thickness were grown by MOCVD on c-plane sapphire substrates [9]. Trimethylboron (TMB) and ammonia (NH_3) were used as precursors for growth and nitrogen was used as a carrier gas. Due the nature of layered structure of h-BN, freestanding *h*-^{10}BN films were obtained by mechanical separation from sapphire substrates. Freestanding *h*-^{10}BN films were sliced into various dimensions to fabricate neutron detectors with varying detection areas. E-beam evaporation was used to deposit bi-layer metal contacts consisting of Ni (10 nm)/Au (20 nm) on both sides of the *h*-^{10}BN film creating a simple vertical "photoconductor-type" device. The most important electrical transport properties pertaining to the performance of detectors were characterized to identify the suitability of the grown h-BN epilayers for detector fabrication. These include current-voltage (I-V) or current density-voltage (J-V) characteristics and photo-generated carrier mobility-lifetime (μτ) products.

Due to its layered structure, h-BN exhibits a strong optical absorption of about 7.5×10^5/cm for the above bandgap photons [25,26], which provides an optical absorption length of only about 14.5 nm [26]. To emphasize the difference in the length scales between the photon and thermal neutron absorption lengths, Fig. 1(b) plots the absorption probability of above bandgap photons in *h*-BN. It can be seen clearly that the incoming above bandgap photons will be completely absorbed within 70 nm (~5λ) of the illuminated surface of *h*-BN, whereas a thickness exceeding 200 μm is needed to absorb 100% incoming thermal neutrons. This unique property enables us to characterize electrical transport properties such as μτ products for holes and electrons separately, as illustrated in Fig. 2. Depending upon the polarity of illuminated surface specific charge carrier (hole or electron) can be selected for charge transport in the vertical direction. Positively (negatively) biased illuminated surface collects photo-generated electrons (holes) and therefore, allows only holes (electrons) to transport between the electrodes. Photoluminescence (PL) emission spectra were measured to reveal relative emission peak intensities of band edge vs impurity transitions to assess relative concentrations of undesired defects in materials grown under different conditions. The PL measurement system used consists of a pulsed (76 MHz repetition rate and 100 fs pulse width) frequency-quadruped Ti-sapphire laser with an excitation wavelength at 195 nm and average optical power of ~ 1 mW, a monochromator (1.3 meters), a microchannel plate photomultiplier tube, and a closed-cycle He refrigerator with a temperature range between 10 - 850 K.

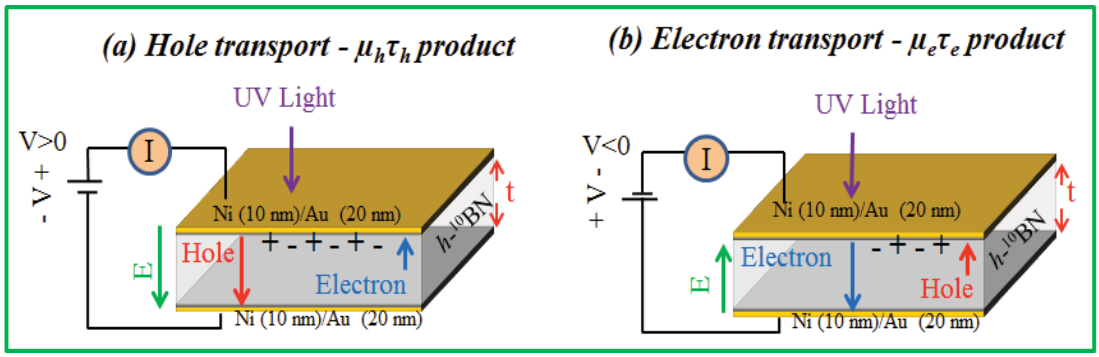

Figure 2. Schematics of cross-sectional views and bias scenarios for measuring the mobility-lifetime products the (a) hole transport and (b) electron transport in thick *h*-BN epilayers.

3. RESULTS AND DISCUSSION

3.1. Electrical transport properties characterization

Detectors were fabricated from two different *h*-^{10}BN samples, sample A and sample B, of 43 μm and 50 μm in thicknesses respectively. Sample A (43 μm thick) has been used to fabricate 1 mm × 1 mm neutron detectors with a detection efficiency of about 51% at a bias voltage of 400 V [9]. PL emission spectra revealed that the donor-acceptor pair transition at about 4.1 eV [31] associated with nitrogen vacancy (V_N) shallow donors and deep level acceptors associated with carbon impurities occupying on nitrogen sites (C_N) is stronger in sample A than in sample B, indicating that the concentrations of V_N and C_N in sample A are higher than those in sample B. V_N and C_N are known to be two of the most common impurities in *h*-BN [32-39]. Conducting epitaxial growth of *h*-BN in nitrogen-rich conditions appears to be an effective approach in minimizing native defects (e.g., V_N) and point (e.g., C_N) defects [31], which are potential charge carrier traps. Therefore, sample B is expected to have a better overall material quality over that of sample A. Figure 3 compares the dark J-V characteristics of detectors fabricated from sample A and sample B. The dark current density (or leakage current density) in sample B is ~0.1 nA/cm^2 at a bias voltage of 500 V, which is nearly one order of magnitude lower than that of sample A. The measured resistivity (ρ) of sample B (~3.5 × 10^{14} Ω cm) is about

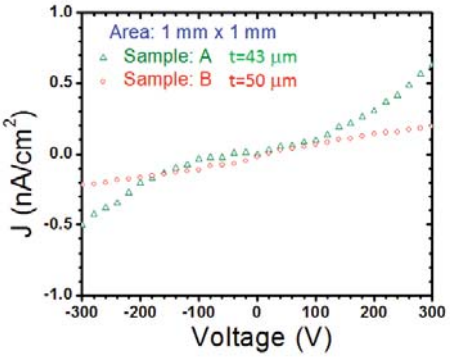

Figure 3. Dark (leakage) current density vs applied voltage (or J-V characteristics) of 1 mm^2 neutron detectors fabricated from sample A (43 μm thick freestanding ^{10}B enriched *h*-BN epilayer) and from sample B (50 μm thick freestanding ^{10}B enriched *h*-BN epilayer).

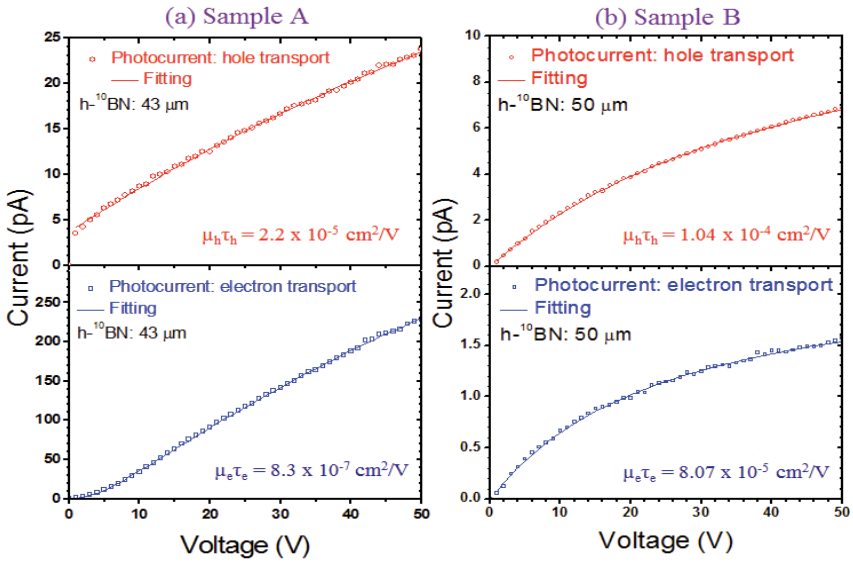

Figure 4. Photocurrent characteristics of (a) a 1 mm^2 neutron detector fabricated from sample A (43 μm thick freestanding ^{10}B enriched *h*-BN epilayer) and (b) a 1 mm^2 neutron detector fabricated from sample B (50 μm thick freestanding ^{10}B enriched *h*-BN epilayer) for hole transport (top) and electron transport (bottom). The solid curves are the least squares fitting of data with Eq. (4).

5 times larger than that of sample A (~0.7×10^{14} Ω cm). The results clearly indicate that the overall material quality of sample B is improved over that of sample A, consistent with the PL results.

Figure 4 compares the photocurrents of two 1 mm × 1 mm devices fabricated from sample A and B. Fitting the photocurrents obtained in the configurations of Fig. 2(a) and Fig. 2(b), corresponding to hole and electron transport, respectively, using the Many's equation [40] below allows us to obtain the μτ-products for holes and electrons:

$$I_i(V) = I_{0,i}\left[\frac{V\mu_i\tau_i\left(1 - e^{-\frac{L^2}{V\mu_i\tau_i}}\right)}{L^2\left(1 + \frac{s_i L}{\mu_i V}\right)}\right], \quad (i = e, h) \tag{4}$$

Here, I_0 is the saturation current, and $\mu_e\tau_e$ ($\mu_h\tau_h$) and s_e (s_h) denote the mobility-lifetime product and surface recombination velocity for electrons (holes), respectively. The results reveal that $\mu_h\tau_h$ is greater than $\mu_e\tau_e$ for both sample A and sample B. This is consistent with our understanding that although μ_h and μ_e are comparable, τ_h is larger than τ_e, implying that holes act as the majority carriers in undoped h-BN [9]. For a given device dimension, enhancing the μτ product would reduce the bias voltage (V) required for charge collection as well as the associated leakage current. This is because most charge carriers generated inside the detector can be collected at the electrodes when the condition of recombination time (τ) ≥ transit time (τ_t) is satisfied, i.e., $\mu\tau \geq L^2/V$ ($\tau_t = L/\mu E, E = V/L$), where V is the applied voltage and L the transit length (the thickness of the detector in the present case). The results presented in Fig. 4 showed that both $\mu_e\tau_e$ and $\mu_h\tau_h$ of sample B are almost one order of magnitude larger than those of sample A. Additionally, the fitted values of s/μ from 1 mm² detectors are $s_h/\mu_h = 9.6 \pm 0.2 \times 10^3$, $s_e/\mu_e = 4.9 \pm 0.2 \times 10^3$ and $s_h/\mu_h = 1.1 \pm 0.3 \times 10^4$ V/cm, $s_e/\mu_e = 8.6 \pm 0.3 \times 10^3$ V/cm for sample B and sample A respectively. These results again corroborates the fact that the overall material quality of sample B is improved over that of sample A.

To further calibrate the suitability of sample A and sample B for detector fabrication, we have measured the pulse height spectra of 1 mm × 1 mm devices fabrication from sample A and sample B in absence of any sources. The pulse height spectra shown in Fig. 5 were obtained by recording the dark counts for 8 hours with the devices biased at 200 V. The results revealed that the dark counts is almost one order of magnitude higher for the 1 mm × 1 mm detector fabricated from sample A than the 1 mm × 1 mm detector fabricated from sample B, which again confirm that the sample B has a better overall material quality than sample A. This high background noise related to the high dark counts limits the ability of scaling up the device size while maintaining an equal level of detection efficiency for detectors fabricated from sample A. Based on the observed results of one order of magnitude reduction in the dark counts shown in Fig. 5 as well as in the leakage current density shown in Fig. 2, we fabricated 3 mm × 3 mm detectors from sample B which possess one order of magnitude enhancement in the device area over the previous achievement [9].

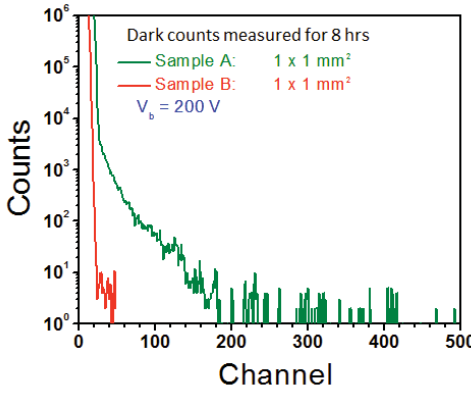

Figure 5. Dark pulse height spectra of 1 × 1 mm² detectors fabricated from sample A (t=43 μm) and sample B (t=50 μm) measured under a bias voltage of 200 V for 8 hours in absence of any sources.

3.2. Thermal neutron detection efficiency measurements

A Californium-252 (^{252}Cf) neutron source with a radioactivity of 0.77 mCi (~ 3.29×10^6 n/s) moderated

by a 1-inch thick HDPE moderator was used to provide thermal neutrons as described in earlier works [9,10,41]. Detection electronics were commercially obtained from Cremat Inc. and included a charge sensitive preamplifier and a Gaussian-shaping amplifier. A Gaussian shaped pulse is fed into a multichannel analyzer (MCA) (Amptek 8000D) to obtain the pulse height spectrum of the reaction conceived inside the *h*-BN detector. Analog amplifiers are shielded from electronic noise inside an aluminum box along with the detector. A preamplifier (mode CR-110) is chosen for maximum amplification of the signal with minimum noise induction. A Gaussian shaping amplifier (model CR-200) with a 2 μs shaping time (FWHM 4.7 μs) is used for further amplification and pulse shape optimization. The experiment was set up in such a way that the detector to source distance was 60 cm (or 57.5 cm from the front surface of the moderator) as depicted in Fig. 6(a). The pulse height spectrum of the neutron response of our 3 × 3 mm^2 size detector was recorded at a bias voltage of 200 V for 15 minutes and is shown in Fig. 6(b). The corresponding "dark" response was also measured without any radiation exposure under the same conditions. Gamma exposure from Caesium-137 (^{137}Cs) confirmed unresponsiveness of *h*-BN detectors to gamma photons [9].

Neutrons are counted one at a time due to the very low rate of incident neutrons on the detector compared to the response time of the detection system with a FWHM of the output Gaussian pulse of 4.7 μs. Daughter particles (Li and α particles) produced from the nuclear reaction travel inside the *h*-BN film subsequently generating electron-hole clouds on their way. Li and α particles both have short ranges (about 2 μm for Li and about 5 μm for α [42]) in *h*-BN compared to device thickness and therefore deposit all their energies inside *h*-BN. When applied electric field in the detector is sufficiently strong, most charge carriers are collected on the electrodes within a very short time, which is integrated in the charge sensitive preamplifier generating a voltage pulse at the output. This voltage pulse is then amplified and shaped in Gaussian shaping amplifier. Each pulse therefore corresponds to one neutron absorbed and placed at a certain channel by the MCA.

The total neutron count was obtained by integrating the spectrum beyond the highest channel of dark

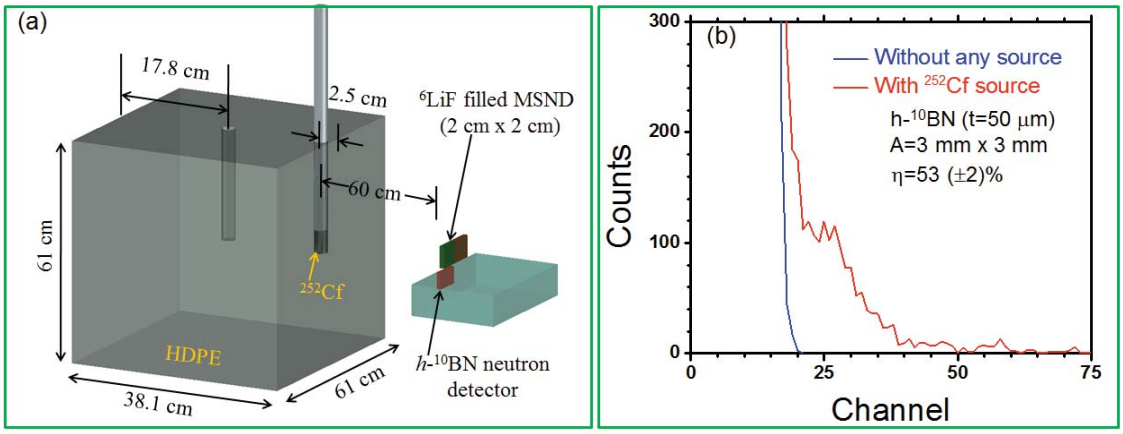

Figure 6. (a) Schematic diagram of the experimental setup for thermal neutron response pulse height spectra and detection efficiency measurements. ^{252}Cf source is placed in the outer hole of a HDPE moderator, 2.5 cm away from the surface of the HDPE moderator. The distance from ^{252}Cf source to *h*-^{10}BN detector as well as to ^{6}LiF filled MSND is fixed at 60 cm. (b) Pulse height spectrum of a 3 × 3 mm^2 detector fabricated from sample B of *h*-^{10}BN of thickness 50 μm measured under a bias voltage of 200 V for 15 minutes. Red curve indicates response under thermal neutron irradiation. Blue curve indicates the background counts in the absence of any source [43].

response, which effectively acted as a low-level discriminator (LLD). Count rate obtained in this way was 1.7 ± 0.01 n/s, giving a count rate per unit area of 18.4 ± 0.2 n/s cm^2. Thermal neutron response of the *h*-^{10}BN detector was calibrated against a commercially purchased ^{6}LiF filled microstructured semiconductor neutron detector (MSND) from Radiation Detection Technologies, Inc. This MSND (Domino™ V4) of model D411S-30-D0010-V4 has a built-in circuit which produces TTL pulses of amplitude 10 V and places all counts in a single channel. Furthermore, the circuit for MSND also includes a built-in LLD which eliminates any

background counts. It was specified with a detection efficiency of 30 (±1) % for thermal neutrons with a device area of 4 cm^2. A count rate of 42.0 ± 0.13 n/s was obtained from the MSND by placing it at the same position as *h*-^{10}BN detector, providing a count rate per unit area of 10.5 ± 0.03 n/s cm^2. The thermal neutron detection efficiency for the 3 × 3 mm^2 *h*-^{10}BN detector can therefore be deduced from

$$\eta_{^{10}BN} = \frac{C_{^{10}BN}}{C_{MSND}} \times \eta_{MSND} = \frac{18.4(\pm 0.1)}{10.5(\pm 0.03)} \times 30(\pm 1.0)\% = 52.6\ (\pm 2.2)\ \% \quad (5)$$

Here, $C_{^{10}BN}$ and C_{MSND} are count rates per unit area, whereas $\eta_{^{10}BN}$ and η_{MSND} denote the thermal neutron detection efficiency of *h*-^{10}BN and MSN detectors, respectively. The measured detection efficiency of about 53 (± 2)% for our 3 × 3 mm^2 device fabricated from sample B biased at 200 V is in the same level as our previously reported efficiency of about 51% for our 1 × 1 mm^2 detector fabricated from sample A biased at 400 V and however is much higher than a value of about 30% when the 1 × 1 mm^2 detector fabricated from sample A was biased at 200 V. The results suggest that the realization of *h*-BN epilayers with reduced defect concentrations and enhanced resistivity (> 10^{14} Ω cm) and mobility-lifetime products (μτ) is the key to enable the scaling up by one order of magnitude in the detection area while maintaining an equal level of detection efficiency.

4. SUMMARY

Significant progress in MOCVD growth of *h*-BN epilayers has been made. Unintentionally doped ^{10}B enriched *h*-BN epilayers with 50 μm in thickness and an electrical resistivity (ρ) as high as ~3.5 × 10^{14} Ω cm have been achieved. The measured leakage current density of fabricated vertical "photoconductive-like" detectors is as low as ~0.1 nA/cm^2 at a bias voltage of 500 V. These improvements have resulted in the realization of *h*-BN neutron detectors possessing one order of magnitude enhancement in the detection area but maintaining an equal level of detection efficiency of prior achievement at about 53%. The work laid the foundation for realizing large area detectors. Due to the fact that the band gap of *h*-BN is about 6.5 eV, the electrical resistivity of intrinsic h-BN is expected to exceed 10^{20} Ω·cm. Therefore, further increase in the electrical resistivity of *h*-BN is anticipated as the epitaxial growth processes further advance to provide further improvements in material quality, which ultimately will enable the fabrication of large size (> 1 cm × 1 cm) and high sensitivity *h*-BN neutron detectors.

ACKNOWLEDGEMENTS

DOE NNSA SSAA program (DE-NA0002927) supported the research efforts on *h*-BN neutron detector fabrication. The study of the basic transport properties of *h*-BN is made possible by the support from ARO (W911NF-16-1-0268) and monitored by Dr. Michael Gerhold. Jiang and Lin are grateful to the AT&T Foundation for the support of Ed Whitacre and Linda Whitacre Endowed chairs.

REFERENCES

a) hx.jiang@ttu.edu

[1] Q. Shao, L. F. Voss, A. M. Conway, R. J. Nikolic, M. A. Dar, and C. L. Cheung, Appl. Phys. Lett. **102**, 063505 (2013).

[2] A. M. Conway, R. J. Nikolic, and T. F. Wang, Proceedings of the International Semiconductor Device Research Conference, IEEE, New York, pp. 589 (2007).

[3] K-C Huang, R. Dahal, J. J.-Q. Lu, A. Weltz, Y. Danon, and I. B. Bhat, Nucl. Instr. Meth. Phys. Res. A **763**, 260 (2014).

[4] S. L. Bellinger, R. G. Fronk, W. J. McNeil, T. J. Sobering, and D. S. McGregor, IEEE Trans. Nucl. Sci. **59**, 167 (2012).

[5] K. Osberg, N. Schemm, S. Balkir, J. O. Brand, M. S. Hallbeck, P. A. Dowben, and M. W. Hoffman, IEEE Sensor J. **6** 1531 (2006).
[6] D. S. McGregor, T. C. Unruh, and W. J. McNeil, Nucl. Instr. Meth. Phys. Res. A **591**, 530 (2008).
[7] A. N. Caruso, J. Physics: Condensed Matter **22**, 443201 (2010).
[8] J. Li, R. Dahal, S. Majety, J. Y. Lin, and H. X. Jiang, Nucl. Instrum. Methods Phys. Res., Sect. A **654**, 417 (2011).
[9] A. Maity, T. C. Doan, J. Li, J. Y. Lin, and H. X. Jiang, Appl. Phys. Lett. **109**, 072101 (2016).
[10] K. Ahmed, R. Dahal, A. Weltz, James J.-Q. Lu, Y. Danon, and I. B. Bhat, Appl. Phys. Lett. **110**, 023503 (2017).
[11] G. F. Knoll, "Radiation detection and measurement," 4th edition, (John Wiley & Sons, 2010).
[13] B. Arnaud, S. Lebègue, P. Rabiller, and M. Alouani, Phys. Rev. Lett., **96**, 026402 (2006) and **100**, 189702 (2008).
[14] L. Wirtz, A. Marini, and A. Rubio, Phys. Rev. Lett. **96**, 126104 (2006).
[15] L. Museur, G. Brasse, A. Pierret, S. Maine, B. Attal-Tretout, F. Ducastelle, A. Loiseau, J. Barjon, K. Watanabe, T. Taniguchi, and A. Kanaev, Physica Status Solidi (RRL), **5**, 214 (2011).
[16] L. Museur, E. Feldbach, and A. Kanaev, Phys. Rev. B **78**, 155204 (2008).
[17] K. Watanabe and T. Tanniguchi, Phys. Rev. B **79**, 193104 (2009).
[18] M. G. Silly, P. Jaffrennou, J. Barjon, J. S. Lauret, F. Ducastelle, A. Loiseau, E. Obraztsova, B. Attal-Tretout, and E. Rosencher, Phys. Rev. B **75**, 085205 (2007).
[19] X. K. Cao, B. Clubine, J. H. Edgar, J. Y. Lin, and H. X. Jiang, Appl. Phys. Lett. **103**, 191106 (2013).
[20] Y. Kubota, K. Watanabe, O. Tsuda and T. Taniguchi, Science **317** 932 (2007).
[21] K. Watanabe, T. Taniguchi, T. Niiyama, K. Miya, and M. Taniguchi, Nature Photonics, **3**, 591 (2009).
[22] K. Watanabe, T. Taniguchi and H. Kanda, Nature Materials **3**, 404 (2004).
[23] R. Dahal, J. Li, S. Majety, B. N. Pantha, X. K. Cao, J. Y. Lin, and H. X. Jiang, Appl. Phys. Lett. **98**, 211110 (2011).
[24] S. Majety, J. Li, X. K. Cao, R. Dahal, B. N. Pantha, J. Y. Lin, and H. X. Jiang, Appl. Phys. Lett. **100**, 061121 (2012).
[25] T. Sugino, K. Tanioka, S. Kawasaki, and J. Shirafuji, Jpn. J. Appl. Phys. **36**, L463 (1997).
[26] J. Li, S. Majety, R. Dahal, W. P. Zhao, J. Y. Lin, and H. X. Jiang, Appl. Phys. Lett. **101**, 171112 (2012).
[27] A. K. Geim and I. V. Grigorieva, Nature, **499**, 419 (2013).
[28] N. Alem, R. Erni, C. Kisielowski, M. D. Rossell, W. Gannett, and A. Zettl, Phys. Rev. B **80**, 155425 (2009).
[29] C. R. Dean, A. F. Young, I. Meric, C. Lee, L. Wang, S. Sorgenfrei, K. Watanabe, T. Taniguchi, P. Kim, K. L. Shepard and J. Hone, Nature Nanotechnology **5**, 722 (2010).
[30] T. P. Kaloni, Y. C. Cheng, and U. Schwingenschlögl, J. Mater. Chem. **22**, 919 (2012).
[31] X. Z. Du, J. Li, J. Y. Lin, and H. X. Jiang, Appl. Phys. Lett. **106**, 021110 (2015).
[32] W. Orellana and H. Chacham, Phys. Rev. B **63**, 125205 (2001).
[33] A. Zunger and A. Katzir, Phys. Rev. **11**, 2378 (1975).
[34] M. Fanciulli and T. D. Moustakas, Physica B **185**, 228 (1993).
[35] I. Jimenez, A. F. Jankowski, L. J. Terminello, D. G. J. Sutherland,J. A. Carlisle, G. L. Doll, W. M. Tong, D. K. Shuh, and F. J. Himpsel, Phys. Rev. B **55**, 12025(1997).
[36] T. B. Ngwenya, A. M. Ukpong, and N. Chetty, Phys. Rev. B **84**, 245425(2011).
[37] B. Huang and H. Lee, Phys. Rev. B **86**, 245406 (2012).
[38] V. Wang, N. Ma, H. Mizuseki, and Y. Kawazoe, Solid State Commun. **152**, 816 (2012).
[39] C. Attaccalite, M. Bockstedte, A. Marini, A. Rubio, and L. Wirtz, Phys. Rev. B **83**, 144115 (2011).
[40] A. Many, J. Phys. Chem. Solids **26**, 575 (1965).
[41] J. Clinton, "Optimization and characterization of a novel shelf powered solid state neutron detector," Ph.D. thesis, Rensselaer Polytechnic Institute, New York, USA, 2011, Chap. 3, pp. 73–78.
[42] F. P. Doty, "Boron nitride solid state neutron detectors," US patent 6,727,504, 2004.
[43] A. Maity, S. J. Grenadier, J. Li, J. Y. Lin, and H. X. Jiang, Appl. Phys. Lett. **111**, 033507 (2017).